ARTICLES
PUBLISHED ONLINE: 10 JUNE 2012 | DOI: 10.1038/NCHEM.1381
nature chemistry

The synthesis, crystal structure and charge-transport properties of hexacene

Motonori Watanabe[1], Yuan Jay Chang[1], Shun-Wei Liu[2], Ting-Han Chao[3], Kenta Goto[4], Md. Minarul Islam[1], Chih-Hsien Yuan[1], Yu-Tai Tao[1], Teruo Shinmyozu[4] and Tahsin J. Chow[1]*

Acenes can be thought of as one-dimensional strips of graphene and they have the potential to be used in the next generation of electronic devices. However, because acenes larger than pentacene have been found to be unstable, it was generally accepted that they would not be particularly useful materials under normal conditions. Here, we show that, by using a physical vapour-transport method, platelet-shaped crystals of hexacene can be prepared from a monoketone precursor. These crystals are stable in the dark for a long period of time under ambient conditions. In the crystal, the molecules are arranged in herringbone arrays, quite similar to that observed for pentacene. A field-effect transistor made using a single crystal of hexacene displayed a hole mobility significantly higher than that of pentacene. This result suggests that it might be instructive to further explore the potential of other higher acenes.

Acenes are a class of aromatic hydrocarbons composed of linearly fused benzene rings. They are of contemporary interest from a theoretical point of view[1] as well as a practical standpoint as functional organic materials[2,3]. One of the most attractive features of acenes is their exceptionally narrow HOMO–LUMO bandgap, which leads to a higher conductivity than found in other organic compounds[4]. The hole mobility in single crystals of acenes, measured in an organic field-effect transistor (OFET) across gold electrodes on top of SiO_2, increases with the number of aromatic rings; for example, anthracene ($\mu_{FET} = 0.02\ cm^2\ V^{-1}\ s^{-1}$)[5] < tetracene ($\mu_{FET} = 0.4\ cm^2\ V^{-1}\ s^{-1}$)[6] < pentacene ($\mu_{FET} = 1.4\ cm^2\ V^{-1}\ s^{-1}$)[7].

Although larger acenes have great potential in a wide range of applications, their utility is limited severely by both their low solubility and low stability when in solution. Hexacene, for example, was reported more than 70 years ago[8–10], yet its properties have never been unambiguously described until recently, largely due to its tedious synthesis and low solubility[11,12]. To increase solubility, a series of perifunctionalized derivatives containing silylethynyl[13] and organothio[14] substituents have been synthesized. These types of derivatives, including some based on heptacene[15] and nonacene[16,17], have indeed demonstrated higher solubility and stability in solution.

A synthesis of non-substituted hexacene was recently achieved through the photo-induced expulsion of CO molecules from a diketone precursor, with the product collected by matrix isolation[18,19]. At room temperature, hexacene is stable in this polymer matrix for more than 12 h (ref. 19). However, hexacene crystals could not be obtained by this method. A similar matrix isolation approach has also been used recently for the preparation of non-substituted nonacene[20]. It has been established that the photo-expulsion of CO through diketone precursors proceeds through biradical intermediates[21]. In the case of pentacene, the yield was only 74% ($\tau_T = 48.48 \pm 0.15\ \mu s$) from its diketone precursor[22]. In our earlier studies, we designed a superior method for the preparation of pentacene[23–25], which used a monoketone precursor from which the CO expulsion reaction has been proposed to proceed through a concerted pathway (a hypothesis that has been supported by theoretical models[26]). The yield of pentacene made from this precursor was close to quantitative, and crystals could be collected immediately after the reaction. In this Article, we describe the details of a highly efficient solid-state synthesis of hexacene from a monoketone precursor, compound **1** (Fig. 1). The isolated species has been fully characterized and is found to be stable at temperatures in excess of 300 °C.

Results and discussion

Monoketone precursor **1** was synthesized from commercial materials in five steps in 24% total yield (for synthetic details and characterization see Supplementary Information). It is soluble in common organic solvents such as chloroform and tetrahydrofuran

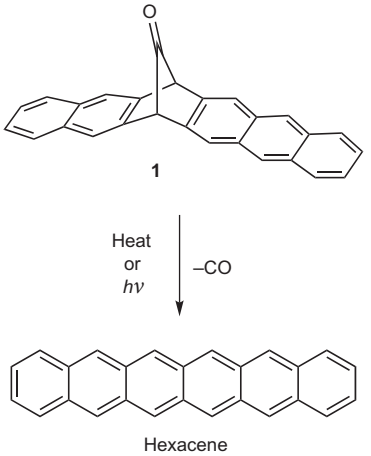

Figure 1 | Generation of hexacene from precursor 1 by CO expulsion. The transformation can be achieved either by heating a solid sample of **1** at 180 °C, or by irradiating a THF solution of **1** at 365 ± 30 nm.

[1]Institute of Chemistry, Academia Sinica, No. 128, Academia Road Sec 2, Nankang, Taipei, 11529, Taiwan, [2]Department of Electronic Engineering, Ming Chi University of Technology, No. 84, Gongzhuan Road, Taishan District, New Taipei City 24301, Taiwan, [3]Department of Chemistry, National Taiwan Normal University, Ting-Chow Road, Taipei, 11677, Taiwan, [4]Institute of Materials Chemistry and Engineering (IMCE), Kyushu University, 6-10-1 Hakozaki, Fukuoka, 812-8581, Japan. *e-mail: tjchow@chem.sinica.edu.tw

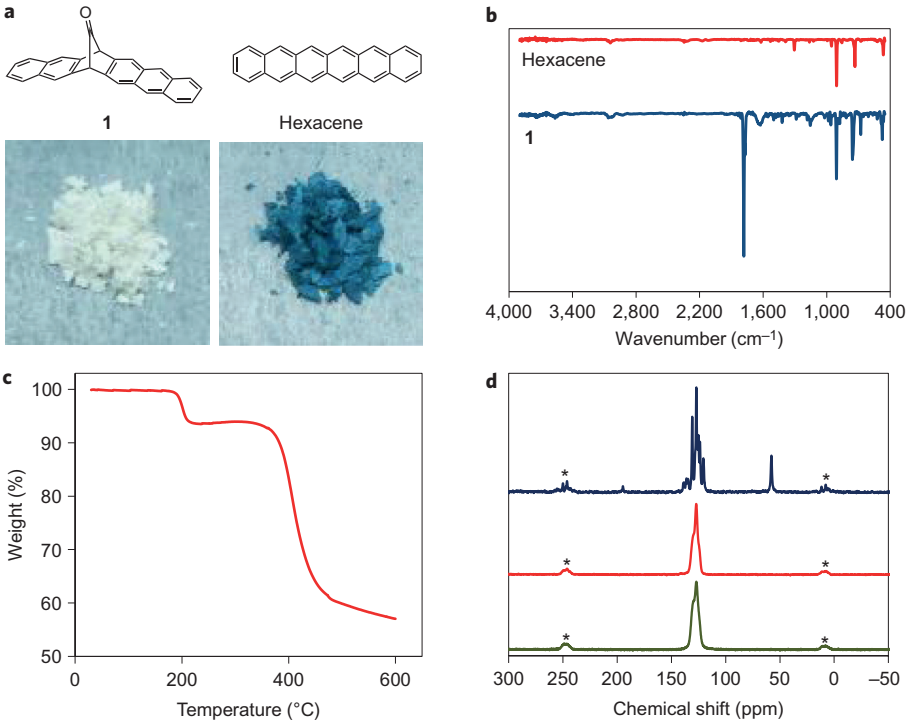

Figure 2 | Characterization of the transformation from 1 to hexacene. a, Physical appearance of **1** (left) and hexacene (right) in the open air. The hexacene was generated by heating **1** at 180 °C in a nitrogen atmosphere. **b**, Infrared spectra of **1** (bottom) and hexacene (top). The diminishing of a characteristic carbonyl peak of **1** at 1,784 cm^{-1} indicates the extent of decarbonylation. **c**, TGA profile of **1**. The weight loss at ~180 °C indicates the formation of hexacene through CO expulsion. **d**, CP-MAS spectra of **1** (top), hexacene produced by heating **1** at 180 °C under a nitrogen atmosphere (middle) and hexacene left at ambient conditions in the dark for 30 days (bottom). Asterisks denote spinning sidebands.

(THF, ~0.3 mg ml^{-1} in both solvents), and the solid can be stored at 5 °C under room light for more than six months.

Compound **1** (2.0×10^{-4} M in THF) displayed the characteristic $^1A \rightarrow {}^1L_a$ transitions of an anthracene chromophore with vibronic progressions at 385 nm ($\log \varepsilon = 3.81$), 365 nm ($\log \varepsilon = 3.96$) and 347 nm ($\log \varepsilon = 3.88$). The conversion of **1** to hexacene was first attempted using a photochemical method. When a THF solution was irradiated at 365 ± 30 nm (12.5 mW cm^{-2} ultraviolet under oxygen-free conditions), the absorption bands of **1** diminished, accompanied by the growth of new bands at 667, 611 and 557 nm (shoulder) corresponding to the vibronic progressions of a π–π^* transition of hexacene[11,18,19]. However, these new bands persisted only briefly then disappeared, probably due to dimerization (Supplementary Fig. S7)[19].

The conversion was also attempted by heating solid **1** to ~180 °C in a nitrogen atmosphere. Under these conditions, the colour changed rapidly from white to blue-green (Fig. 2a). During the thermal transformation, the characteristic carbonyl peak of **1** at 1,784 cm^{-1} diminished (Fig. 2b). The high-resolution matrix-assisted laser desorption/ionization–time of flight (MALDI–MS) spectrum indicated a molecular ion signal at m/z 329.1341 (MH^+, calcd 329.1330, error = 3.0 ppm), corresponding to hexacene (Supplementary Fig. S9).

Thermal gravimetric analysis (TGA) of **1** was carried out with a scan rate of 10 °C min^{-1} under nitrogen flow (Fig. 2c). A weight loss of 6.6% (calcd 7.9%) occurred at ~180 °C, corresponding to the formation of hexacene through CO expulsion. The sample then remained stable over a wide temperature range until ~330 °C, when another weight loss occurred due to vaporization. The nature of hexacene was also examined by solid-state cross-polarization magic angle spinning (CP-MAS) NMR spectroscopy. The spectrum of compound **1** showed three absorption bands at δ 57.7 ppm (bridgehead), 120–139 ppm (aromatic) and 194.7 ppm (carbonyl) (Fig. 2d). After thermal conversion, the bridgehead and carbonyl peaks faded away and left behind only the aromatic ones at 121–134 ppm. The absence of any other signals in the spectrum indicates that the transformation proceeded cleanly. A simulated spectrum calculated by density function theory (DFT) B3LYP/6-311+G(2d,p)//M06/6-31G(d) matched well with the experimental results (Supplementary Fig. S11).

After being exposed to air at room temperature for 24 h in the dark, the hexacene gave virtually the same CP-MAS NMR spectra, indicating the high stability of hexacene under ambient conditions. Further evidence of its high stability was provided by solid-state absorption spectra. A THF solution of **1** was spincast on a quartz plate (transparency >98% at a wavelength of 380 nm) into a 200-nm-thick film, which was converted to hexacene by heating at 180 °C under a nitrogen atmosphere. The film of **1** before heating displayed the characteristic feature of anthracene at 403 nm (3.08 eV, Supplementary Fig. S8). After heating, the band disappeared, accompanied by the growth of new peaks at 840 nm (1.48 eV), 765 nm (1.62 eV), 708 nm (1.75 eV) and 654 nm (1.90 eV) (Fig. 3a). The low energy peaks were redshifted with respect to those in a THF solution at 667 nm (1.86 eV), and can be rationalized by the effect of Davydov splitting[27–29]. The peaks at 840 nm (1.48 eV) and 765 nm (1.62 eV) were assigned to the Davydov doublet of the 0–0 band, and those at 708 nm (1.75 eV) and 654 nm (1.90 eV) to the Davydov doublet of the 0–1 band. The hexacene film was stable for more than one month, when it was left in air at room temperature in the dark, as indicated by both the CP-MAS NMR spectra (Fig. 2d) and the absorption spectra (Supplementary Fig. S12).

In an earlier report it was shown that hexacene in a polymethyl methacrylate (PMMA) matrix reacted gradually with dioxygen, which diffused slowly into the matrix, under irradiation from an ultraviolet LED array (395 ± 25 nm)[19]. For comparison, the photochemical stability of a hexacene thin film was investigated by exposing it to ultraviolet light at 365 nm ($\pm$30 nm using a

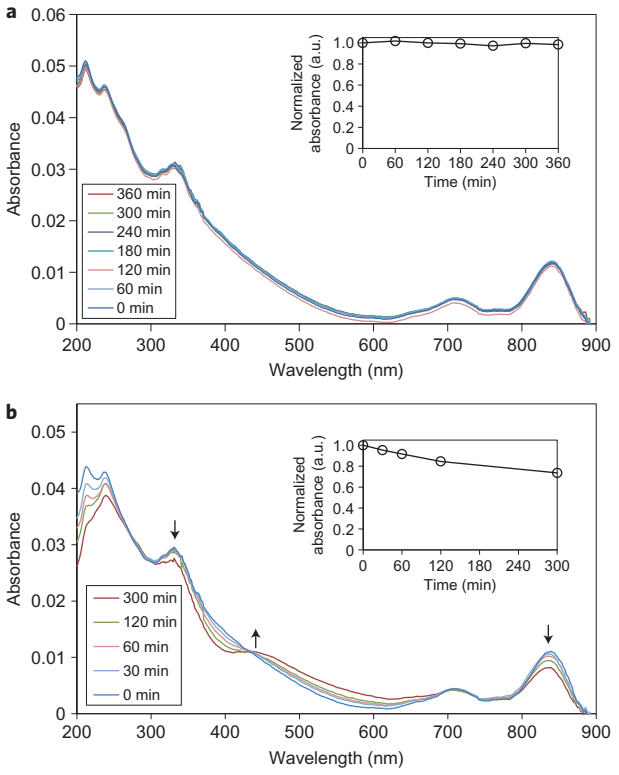

Figure 3 | Absorption spectra of hexacene thin films. a, Spectra of a thin film of hexacene measured in the dark under ambient conditions. Inset: time dependence plot of relative intensity at 840 nm from 0 to 360 min. There is no observable change of intensity, indicating that the thin film of hexacene is stable. **b**, Spectra after ultraviolet irradiation at 365±30 nm (ultraviolet lamp, 12.5 mW cm^{-2}, black light >400 nm filtered) in air. Inset: time dependence plot of relative absorption intensity at 840 nm from 0 to 300 min. The decay of intensity clearly shows that hexacene has undergone a structural change.

12.5 mW cm^{-2} black-light ultraviolet lamp, >400 nm filtered) in air. The absorption intensity of hexacene decreased gradually, accompanied by an increase of a new band at ~430 nm (Fig. 3b). In the meantime, a new signal was observed in the high-resolution MALDI-MS spectrum, which corresponded to an endoperoxide adduct (m/z 361.1238 (MH^+), calcd 361.1228, error = 2.8 ppm) (Supplementary Fig. S10). These results suggest that hexacene underwent a slow photochemical oxidation in the presence of air[30–32]. A time-dependent measurement of the intensity of the 840 nm band revealed that the amount of photo-oxidation increased steadily at the early stage (that is, from 0 to 120 min), but slowed down substantially after 300 min (Fig. 3b, inset). It is probable that air oxidation proceeded mainly on the surface of the solids and, as time went by, it became more difficult for oxygen to penetrate into the interior of the sample. The photo-ionization energy of a hexacene thin film was measured by photoemission yield spectroscopy (AC-2 Riken), and it was found that the HOMO level of hexacene (−4.96 eV) is higher than that of pentacene (−5.14 eV)[33]. The LUMO level of a thin film (−3.56 eV) was then deduced by subtracting the HOMO from the edge of the absorption band (889 nm, 1.40 eV) (Supplementary Fig. S13).

The ultimate structural proof came from the single-crystal structure determined by X-ray diffraction analysis. Pure hexacene was obtained using the physical vapour-transport (PVT) method[34]. A sample of precursor **1** was heated at 180 °C in a nitrogen atmosphere to give a sizable amount of pure hexacene. It was then transferred into a glass tube for PVT, and the tube was heated in an oven at 260–300 °C with a flow of argon gas (20–40 ml min^{-1}). Blue-green platelet crystals were collected from a temperature gradient zone inside the glass tube. A single crystal was selected and subjected to X-ray diffraction analysis. Crystal parameters were collected at −150 °C in the dark. The crystal belongs to the triclinic space group $P-1$, with $a = 6.292$, $b = 7.673$, $c = 16.424$ Å, $\alpha = 98.66°$, $\beta = 91.16°$ and $\gamma = 95.71°$. The molecules are shown to be packed in herringbone arrays, quite analogous to pentacene (Fig. 4). The result was consistent with expectations (triclinic crystal of space group $P-1$), with only a slight variation in the unit cell dimension ($a = 7.9$, $b = 6.1$, $c = 18.4$ Å, $\alpha = 102.7°$, $\beta = 112.3°$ and $\gamma = 83.6°$)[12].

The herringbone packing motif is believed to be responsible for the high stability of hexacene in the solid state. Compared to the hexacene derivatives with silylethynyl substituents (for example, tri-isobutylsilylethynylhexacene, TIBS-hexacene)[13], the non-substituted hexacene in the crystal exhibited a very slow rate of dimerization. In the crystal of TIBS-hexacene, adjacent molecules are arranged in a shifted face-to-face π-stacking motif, a geometry that is more likely to favour dimerization. In the herringbone packing of non-substituted hexacene, the adjacent molecules are stacked in an edge-to-face manner, which is not suitable for dimerization. It is well known that the electronic properties of acenes depends heavily on their molecular packing patterns. Based on crystal data, the transfer integrals of naphthalene[35], anthracene[36], tetracene[37], pentacene[38] and hexacene were compared. The results showed that hexacene has a much smaller reorganization

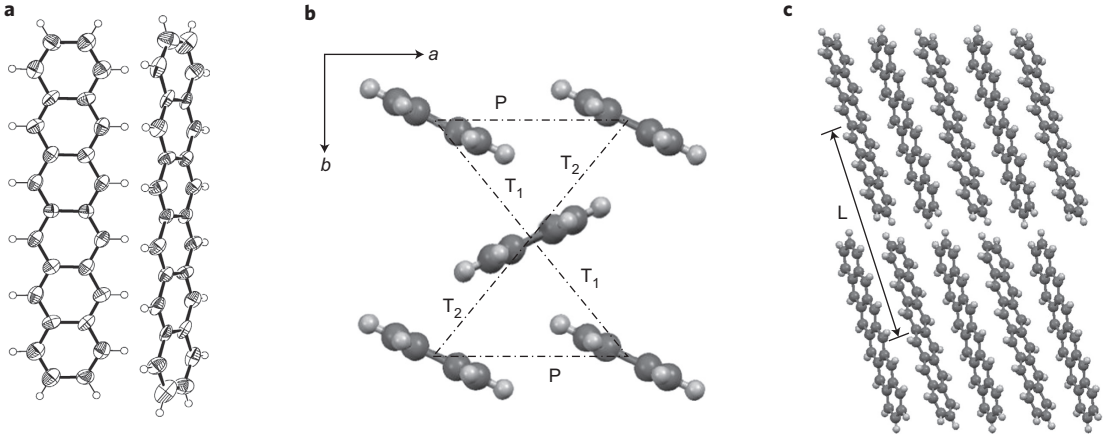

Figure 4 | X-ray crystallographic analysis of hexacene. a, ORTEP drawing of two adjacent hexacene molecules. **b**, Layer arrangement of hexacene molecules on the *a*–*b* plane. **c**, Arrays of hexacene along the *a*-axis. Distances used for computation of transfer integrals are denoted as T_1 and T_2 for transverses, P for parallel and L for longitudinal.

Table 1 | Calculated hole-transporting properties.

Compound	HOMO* (eV)	λ^{+}* (meV)	R (Å), t^{+} (meV)†				μ^{+}‡ (cm^2 V^{-1} s^{-1})
			T_1	T_2	P	L	
Naphthalene[§]	−5.80	183	5.01, 8	5.01, 8	5.93, 36	8.64, 0	0.0511
Anthracene[‖]	−5.24	138	5.22, 19	5.22, 19	6.01, 42	11.12, 0	0.158
Tetracene[¶]	−4.87	113	4.77, 70	5.13, 22	6.06, 37	13.44, 1	0.470
Pentacene[#]	−4.61	95	4.76, 79	5.21, 45	6.27, 31	16.11, 1	0.832
Hexacene	−4.42	79	4.72, 88	5.22, 60	6.31, 37	18.61, 1	1.461

*B3LYP/6-31G(d,p) level; †PW91/DZ2P level calculated at 300 K (t^{+} is given as absolute value); ‡Averaged value along the four directions (T_1, T_2, P and L) under consideration; §Ref. 35; ‖Ref. 36; ¶Ref. 37; #Ref. 38.

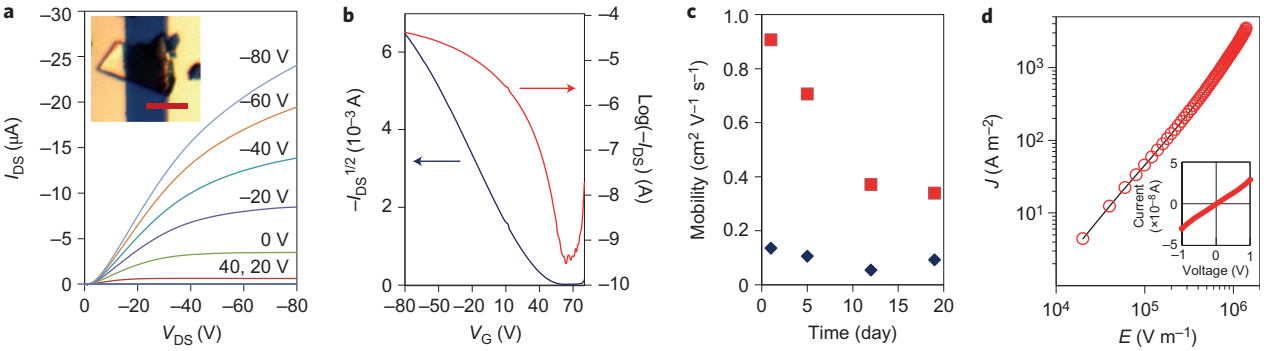

Figure 5 | Single-crystal OFET and conductivity characteristics of hexacene. a, Output characteristics (D, drain; S, source). Inset: a crystal across the electrodes (scale bar, 50 μm) with $W/L = 1.10$. **b**, Transfer characteristics recorded at $V_{DS} = -80$ V (G, gate). **c**, Time-dependent decay of performance under ambient conditions (red squares) and in a nitrogen atmosphere (blue diamonds). **d**, Plot of current J versus electric field E of a hexacene crystal across gold electrodes under ambient conditions. Inset: I–V plot at low voltage (−1 to 1 V).

energy (λ^{+}) and a higher electronic coupling (t^{+}) along both T_1 and T_2 directions (Fig. 4), so a significantly higher hole mobility (μ^{+}) than other acenes was expected (Table 1). The hole mobility can be fitted well by an equation related to the number of aromatic rings, ax^b ($x = 2$–6) (Supplementary Fig. S14). The calculations also suggest that the hole mobility of hexacene is most efficient along the a–b plane.

FETs were then fabricated using single crystals of hexacene. The crystals were grown on a SiO_2/silicon substrate, which was coated with a self-assembled monolayer (SAM) of octyltrichlorosilane (OcTS) and placed inside the PVT tube[39–41]. After crystal growth, gold source and drain electrodes were thermally deposited on top of the substrate through a shadow mask. The averaged performance of 14 independent devices was 0.88 cm^2 V^{-1} s^{-1}, with a threshold at 34 V and an on/off ratio of ~1×10^4 to 1×10^6. Among the results, the best mobility was 4.28 cm^2 V^{-1} s^{-1}, with an on/off ratio of 1×10^5 and threshold of 37 V (Fig. 5a,b and Supplementary Fig. S15). These FET devices could function effectively for more than 19 days without encapsulation. During this time, a device was kept in an ambient environment under room light and the mobility was observed to reduce gradually from 0.906 cm^2 V^{-1} s^{-1} to 0.339 cm^2 V^{-1} s^{-1} (63% decay). When stored in a nitrogen atmosphere, the mobility reduced from 0.135 cm^2 V^{-1} s^{-1} to 0.092 cm^2 V^{-1} s^{-1} (32% decay, Fig. 5c). This decay is believed to be caused by air oxidation on the surface of the crystal.

It is well known that the performance of transistors depends significantly on the nature of the gate dielectric[39,40]. The hole mobility of pentacene has been reported to be in the range ~0.1–1.4 cm^2 V^{-1} s^{-1} for a single crystal[7,42], ~3.4 cm^2 V^{-1} s^{-1} for a thin film on top of SiO_2 (ref. 43) and ~0.25–15 cm^2 V^{-1} s^{-1} in the presence of other types of surface treatments[44–48]. In this study the hole mobility of a single-crystal hexacene FET was better than that of the best pentacene FETs on top of SiO_2 with OcTS SAM treatment. For comparison, a single crystal of pentacene fabricated in an identical manner to a hexacene crystal demonstrated a hole mobility of 1.2 cm^2 V^{-1} s^{-1} with an on/off ratio of 3×10^6 and threshold at −7 V (Supplementary Fig. S16). The conductivity of crystalline hexacene was also measured under gate-free conditions. Deduced from the J–E plot (Fig. 5d), the conductivity of crystalline hexacene was estimated to be 2.21×10^{-4} Sm^{-1} ($V_{ds} = 1$ V), which is slightly higher than that of pentacene (~2.13×10^{-5} Sm^{-1} to ~2.13×10^{-6} Sm^{-1}) (Fig. 5d)[49,50].

Conclusions

We have developed a highly efficient solid-state synthesis of hexacene. The method involves thermal degradation of a monoketone precursor of hexacene that avoids biradical intermediates. The reaction was conducted in the dark to minimize the possibility of photo-induced oxidation and/or dimerization. Pure hexacene thus prepared can be stored under ambient conditions in the dark for more than one month. Platelet single crystals were obtained by PVT. X-ray diffraction analysis indicated that hexacene molecules are aligned in herringbone arrays, just like pentacene. The OFET devices made with single crystals of hexacene displayed the highest hole mobility of 4.28 cm^2 V^{-1} s^{-1} with an on/off ratio of 1×10^5 and a threshold voltage of 37 V. These devices can function under an ambient environment for more than 19 days. The conductivity of solid-state hexacene was estimated to be 2.21×10^{-4} Sm^{-1}. The nature of pure hexacene was characterized successfully for the first time. It can be concluded that solid-state hexacene is thermally stable up to ~300 °C in the dark, but highly vulnerable in solutions under light.

Methods

General experimental details, synthesis and characterization for all compounds, details of fabrication, theoretical calculations for simulated NMR spectra, and hole mobility characteristics can be found in the Supplementary Information. The synthesis of hexacene from its monoketone precursor **1** is described here, together with the procedures for preparing the single-crystal transistors with hexacene.

Synthesis of hexacene from the monoketone precursor. Precursor **1** was heated at 180 °C for 3 min in a glass container under an inert atmosphere (nitrogen or argon). The colour changed rapidly from white to blue-green during heating, after which a powder of hexacene was obtained in nearly quantitative yield. Crystals of hexacene were obtained using the PVT method. The hexacene powder was

transferred into the glass tube for PVT, and the tube was heated in an oven at 260–300 °C with a flow of argon gas (20–40 ml min^{-1}). Platelet crystals were collected at a temperature gradient zone inside the glass tube. Single crystals were collected and subjected to X-ray diffraction analyses.

FET fabricated with a single crystal of hexacene. FETs were fabricated on a heavily doped silicon wafer with a SiO_2 layer (300 nm) in a top-contact geometry. A SiO_2/silicon substrate was first cleaned with oxygen plasma, then dipped into a toluene solution of OcTS (0.1 wt%) for 10 min, rinsed with toluene, and dried with a stream of nitrogen. Crystals of hexacene were grown directly on top of the OcTS/SiO_2/silicon substrate by inserting it into the PVT glass tube in the crystal growth region. A layer of gold (80 nm) was then thermally deposited at a rate of 0.1 nm s^{-1} under a pressure of 8×10^{-6} torr through a shadow mask. Full experimental details and analysis are given in the Supplementary Information.

Received 3 November 2011; accepted 8 May 2012; published online 10 June 2012

References

1. Bendikov, M., Wudl, F. & Perepichka, D. F. Tetrathiafulvalenes, oligoacenenes, and their buckminsterfullerene derivatives: the brick and mortar of organic electronics. *Chem. Rev.* **104,** 4891–4946 (2004).
2. Bao, Z. & Locklin, J. (eds) *Organic Field-Effect Transistors* (CRC Press, 2007).
3. Anthony, J. E. The larger acenes: versatile organic semiconductors. *Angew. Chem. Int. Ed.* **47,** 452–483 (2008).
4. Bendikov, M. *et al.* Oligoacenes: theoretical prediction of open-shell singlet diradical ground states. *J. Am. Chem. Soc.* **126,** 7416–7417 (2004).
5. Aleshin, A. N., Lee, J. Y., Chu, S. W., Kim, J. S. & Park, Y. W. Mobility studies of field-effect transistor structures based on anthracene single crystals. *Appl. Phys. Lett.* **84,** 5383–5385 (2004).
6. De Boer, R. W., Klapwijk, T. M. & Morpurgo, A. F. Field-effect transistors on tetracene single crystals. *Appl. Phys. Lett.* **83,** 4345–4347 (2003).
7. Goldmann, C. *et al.* Hole mobility in organic single crystals measured by a 'flip-crystal' field-effect technique. *J. Appl. Phys.* **96,** 2080–2086 (2004).
8. Marschalk, C. Linear hexacenes. *Bull. Soc. Chim. Fr.* **6,** 1112–1121 (1939).
9. Clar, E. Aromatic hydrocarbons. XXIV. Hexacene, a green simple hydrocarbon. *Ber. Dtsch. Chem. Ges. B* **72B,** 1817–1821 (1939).
10. Bailey, W. J. & Liao, C-W. Cyclic dienes. XI. New syntheses of hexacene and heptacene. Cyclic dienes. XI. New syntheses of hexacene and heptacene. *J. Am. Chem. Soc.* **77,** 992–993 (1955).
11. Angliker, H., Rommel, E. & Wirz, J. Electronic spectra of hexacene in solution (ground state, triplet state, dication and dianion). *Chem. Phys. Lett.* **87,** 208–212 (1982).
12. Champbell, R. B. & Robertson, J. M. The crystal structure of hexacene, and a revision of the crystallographic data for tetracene and pentacene. *Acta Cryst.* **15,** 289–290 (1962).
13. Purushothaman, B., Parkin S. R. & Anthony, J. E. Synthesis and stability of soluble hexacenes. *Org. Lett.* **12,** 2060–2063 (2010).
14. Kaur, I. *et al.* Substituent effects in pentacenes: gaining control over HOMO–LUMO gaps and photooxidative resistances. *J. Am. Chem. Soc.* **130,** 16274–16286 (2008).
15. Kaur, I., Stein, N. N., Kopreski, R. P. & Miller, G. P. Exploiting substituent effects for the synthesis of a photooxidatively resistant heptacene derivative. *J. Am. Chem. Soc.* **131,** 3424–3425 (2009).
16. Kaur, I., Jazdzyk, M., Stein, N. N., Prusevich, P. & Miller, G. P. Design, synthesis, and characterization of a persistent nonacene derivative. *J. Am. Chem. Soc.* **132,** 1261–1263 (2010).
17. Purushothaman, B., Bruzek, M., Parkin, S. R., Miller, A. F. & Anthony, J. E. Synthesis and structural characterization of crystalline nonacenes. *Angew. Chem. Int. Ed.* **50,** 7013–7017 (2011).
18. Mondal, R., Shah, B. K. & Neckers, D. C. Photogeneration of heptacene in a polymer matrix. *J. Am. Chem. Soc.* **128,** 9612–9613 (2006).
19. Mondal, R., Adhikari, R. M., Shah, B. K. & Neckers D. C. Revisiting the stability of hexacenes. *Org. Lett.* **9,** 2505–2508 (2007).
20. Tönshoff, C. & Bettinger, H. F. Photogeneration of octacene and nonacene. *Angew. Chem. Int. Ed.* **49,** 4125–4128 (2010).
21. Mondal, R., Okharimenko, A. N., Shah, K. & Neckers, D. C. Photodecarbonylation of α-diketones: a mechanistic study of reactions leading to acenes. *J. Phys. Chem. B* **112,** 11–15 (2008).
22. Yamada, H. *et al.* Photochemical synthesis of pentacene and its derivatives. *Chem. Eur. J.* **11,** 6212–6220 (2005).
23. Chen, K. Y., Hsieh, H. H., Wu, C. C., Hwang, J. J. & Chow, T. J. A new type of soluble pentacene precursor for organic thin-film transistors. *Chem. Commun.* 1065–1067 (2007).
24. Chuang, T. H. *et al.* Photogeneration and thermal generation of pentacene from soluble precursors for OFET applications. *Org. Lett.* **10,** 2869–2872 (2008).
25. Watanabe, M. *et al.* Solution-processed organic micro crystal transistor based on tetraceno[2,3-*b*]thiophene from a monoketone precursor. *J. Mater. Chem.* **21,** 11317–11322 (2011).
26. Lai, C. H., Li, E., Chen, K. Y., Chow, T. J. & Chou, P. T. Theoretical investigation of cheletroptic decarbonylation reactions. *J. Chem. Theor. Comput.* **2,** 1078–1084 (2006).
27. Davydov, A. S. The theory of molecular excitons. *Sov. Phys. Usp.* **7,** 145–178 (1964).
28. Siebrand, W. & Zgierski, M. Z. in *Springer Series in Solid-State Science* Vol. 49 (eds Reineker, P., Haken, H. & Wolf, H. C.), Part V, 136–144 (Springer, 1983).
29. Miao, Q., Nguyen, T. Q., Someya, T., Blanchet, G. B. & Nuckolls, C. Synthesis, assembly, and thin film transistor of dihydrodiazapentacene: an isostructural motif for pentacene. *J. Am. Chem. Soc.* **125,** 10284–10287 (2003).
30. Stevens, B., Perez, S. R. & Ors, J. A. Photoperoxidation of unsaturated organic molecules. XIV. $O_2{}^1\Delta_g$ acceptor properties and reactivity. *J. Am. Chem. Soc.* **96,** 6846–6850 (1974).
31. Mazur, M. & Blanchard, G. J. Photochemical and electrochemical oxidation reactions of surface-bound polycyclic aromatic hydrocarbons. *J. Phys. Chem. B* **108,** 1038–1045 (2004).
32. Maliakal, A., Raghavachari, K., Katz, H., Chandross, E. & Siegrist, T. Photochemical stability of pentacene and a substituted pentacene in solution and in thin films. *Chem. Mater.* **16,** 4980–4986 (2004).
33. Uda, M. Open counter for low energy electron detection. *Jpn J. Appl. Phys.* **S24**(4), 284–288 (1985).
34. Laudise, R. A., Klic, C., Simpkins, P. G. & Siegrist, T. Physical vapor growth of organic semiconductors. *J. Cryst. Growth* **187,** 449–454 (1998).
35. Capelli, S. C., Albinati, A., Mason, S. A. & Willis, B. T. M. Molecular motion in crystalline naphthalene: analysis of multi-temperature X-ray and neutron diffraction data. *J. Phys. Chem. A* **110,** 11695–11703 (2006).
36. Brock, C. P. & Dunitz, J. D. Temperature dependence of thermal motion in crystalline anthracene. *Acta Crystallogr. C* **46,** 795–806 (1990).
37. Holmes, D., Kumaraswamy, S., Matzger, A. J. & Vollhardt, K. P. C. On the nature of nonplanarity in the [*N*]phenylenes. *Chem. Eur. J.* **5,** 3399–3412 (1999).
38. Mattheus, C. C. *et al.* Polymorphism in pentacene. *Acta Crystallogr. C* **57,** 939–941 (2001).
39. Kobayashi, S. *et al.* Control of carrier density by self-assembled monolayers in organic field-effect transistors. *Nature Mater.* **3,** 317–322 (2004).
40. Yang, S. Y., Shin, K. & Park, C. E. The effect of gate-dielectric surface energy on pentacene morphology and organic field-effect transistor characteristics. *Adv. Funct. Mater.* **15,** 1806–1814 (2005).
41. Onclin, S., Ravoo, B. J. & Reinhoudt, D. N. Engineering silicon oxide surfaces using self-assembled monolayers. *Angew. Chem. Int. Ed.* **44,** 6282–6304 (2005).
42. Takeya, J. *et al.* Field-induced charge transport at the surface of pentacene single crystals: a method to study charge dynamics of two-dimensional electron systems in organic crystals. *J. Appl. Phys.* **94,** 5800–5804 (2003).
43. Yang, H. *et al.* Conducting AFM and 2D GIXD studies on pentacene thin films. *J. Am. Chem. Soc.* **127,** 11542–11543 (2005).
44. Kitamura, M. & Arakawa, Y. Pentacene-based organic field-effect transistors. *J. Phys. Condens. Matter* **20,** 184011 (2008).
45. Butko, V. Y., Chi, X., Lang, D. V. & Ramirez, A. P. Field-effect transistor on pentacene single crystal. *Appl. Phys. Lett.* **83,** 4773–4775 (2003).
46. Roberson, L. B. *et al.* Pentacene disproportionation during sublimation for field-effect transistors. *J. Am. Chem. Soc.* **127,** 3069–3075 (2005).
47. Reese, C., Chung, W. J., Ling, M. M., Roberts, M. & Bao, Z. High-performance microscale single-crystal transistors by lithography on an elastomer dielectric. *Appl. Phys. Lett.* **89,** 202108 (2006).
48. Jurchescu, O. D., Popinciuc, M., Van Wees, B. J. & Palstra, T. M. Interface-controlled, high-mobility organic transistors. *Adv. Mater.* **19,** 688–692 (2007).
49. Jurchescu, O. D., Baas, J. & Palstra, T. M. Effect of impurities on the mobility if single crystal pentacene. *Appl. Phys. Lett.* **84,** 3061–3063 (2004).
50. Parisse, P., Passacantando, M., Picozzi, S. & Ottaviano, L. Conductivity of the thin film phase of pentacene. *Org. Electron.* **7,** 403–409 (2006).

Acknowledgements

The authors thank D.-L.M. Tzou and M.-M. Chen (Academia Sinica) for measuring the CP-MAS ^{13}C NMR spectrum. Computations were carried out using the computer facilities at the Academia Sinica Computing Center. This work was supported by the National Science Council and Academia Sinica in Taiwan.

Author contributions

M.W. designed and performed the experiments and theoretical calculations. Y.J.C. measured and analysed the data. S.W.L. and M.M.I. designed the devices and analysed the data. T.H.C. and C.H.Y. fabricated the devices. K.G. carried out X-ray diffraction analysis on the crystals. M.W., Y.T.T. and T.S. co-wrote the paper. T.J.C. supervised the project.

Additional information

The authors declare no competing financial interests. Supplementary information and chemical compound information accompany this paper at www.nature.com/naturechemistry. Reprints and permission information is available online at http://www.nature.com/reprints. Correspondence and requests for materials should be addressed to T.J.C.